Antarctic Science 26(6), 708–723 (2014) doi:10.1017/S0954102014000261

Features of the glacial history of the Transantarctic Mountains inferred from cosmogenic ^{26}Al, ^{10}Be and ^{21}Ne concentrations in bedrock surfaces

GREG BALCO[1], JOHN O.H. STONE[2], MACIEJ G. SLIWINSKI[2,3] and CLAIRE TODD[4]

[1]*Berkeley Geochronology Center, 2455 Ridge Road, Berkeley, CA 94709, USA*
[2]*Earth and Space Sciences, University of Washington, Seattle, WA 98195, USA*
[3]*Geoscience, University of Wisconsin, Madison, WI 53706, USA*
[4]*Geosciences, Pacific Lutheran University, Tacoma, WA 98447, USA*
balcs@bgc.org

Abstract: This paper describes measurements of concentrations of cosmogenic ^{26}Al, ^{10}Be and ^{21}Ne in quartz from bedrock surfaces in the Transantarctic Mountains where stratigraphic and geomorphic evidence shows that the surfaces were covered by ice in the past, but were not glacially eroded during periods of ice cover. It then explores to what extent this information can be used to learn about past ice sheet change. First, cosmogenic nuclide concentrations in sandstone bedrock surfaces at two sites in the McMurdo Dry Valleys near 77°S are consistent with an equilibrium between nuclide production and loss by surface erosion and radioactive decay. They are most easily explained by a scenario in which: i) sites more than *c.* 100 m above the present ice surface were almost never ice-covered and eroded steadily at 0.5–1.5 m Ma^{-1}, and ii) sites near the present ice margin experienced similar erosion rates when ice-free, but have been covered by cold-based, non-erosive glacier ice as much as half of the time during the past several million years. Nuclide concentrations in granite bedrock at a site in the Quartz Hills near 85°S, on the other hand, have not reached production-erosion equilibrium, thus retaining evidence of the time they were first exposed to the cosmic ray flux. Nuclide concentrations at these sites are most easily explained by 4–6 Ma exposure, extremely low erosion rates of 5–10 cm Ma^{-1} during periods of exposure, and only very short periods of cold-based, non-erosive ice cover.

Received 30 August 2013, accepted 12 March 2014

Key words: aluminium-26, Antarctic, beryllium-10, cosmogenic nuclide geochemistry, neon-21

Introduction

In this paper, we describe measurements of the cosmic ray-produced radionuclides ^{26}Al, ^{10}Be and ^{21}Ne from intermittently glaciated bedrock surfaces in the Transantarctic Mountains. These bedrock surfaces are characteristic of much of the landscape of the Transantarctic Mountains in that geomorphic and stratigraphic evidence shows that they were covered by ice at least once in the past, but the bedrock surfaces themselves lack any evidence of glacial modification and display only features associated with subaerial weathering and granular disintegration (e.g. Sugden *et al.* 1999, 2005, Sugden & Denton 2004). As this relationship implies a polar climate cold enough to sustain only frozen-based and non-erosive glaciers, the geomorphology of these surfaces provides potential constraints on Cenozoic Antarctic climate and ice sheet change (Sugden *et al.* 1999, Sugden & Denton 2004).

The goal of this paper is to attempt to quantify some of these constraints via cosmogenic nuclide measurements. Concentrations of cosmic ray-produced nuclides in rock surfaces reflect a balance between nuclide production during exposure of the surface to cosmic rays, loss of nuclide-enriched surface material due to erosion and, for radionuclides, loss by radioactive decay. The relative importance of these processes varies according to the half-life of the nuclide in question. Thus comparing inventories of different nuclides can help to reconstruct the exposure history of the surface. For example, ^{26}Al and ^{10}Be are produced by cosmic ray bombardment of quartz at a fixed ratio of ^{26}Al/^{10}Be = 6.75, but ^{26}Al decays twice as fast as ^{10}Be. Thus, if a quartz sample experiences a single period of surface exposure, ^{26}Al and ^{10}Be concentrations are uniquely related to the exposure time by their production ratio and decay constants. If this period of exposure is interrupted by periods during which the sample is shielded from the cosmic ray flux, the ^{26}Al inventory will decay faster than ^{10}Be during these periods, thus the ^{26}Al/^{10}Be ratio will no longer conform to this relationship. Thus, disequilibrium between ^{26}Al and ^{10}Be concentrations can be used to identify surfaces that have experienced complex exposure histories (Klein *et al.* 1986, Nishiizumi *et al.* 1986, Lal 1991).

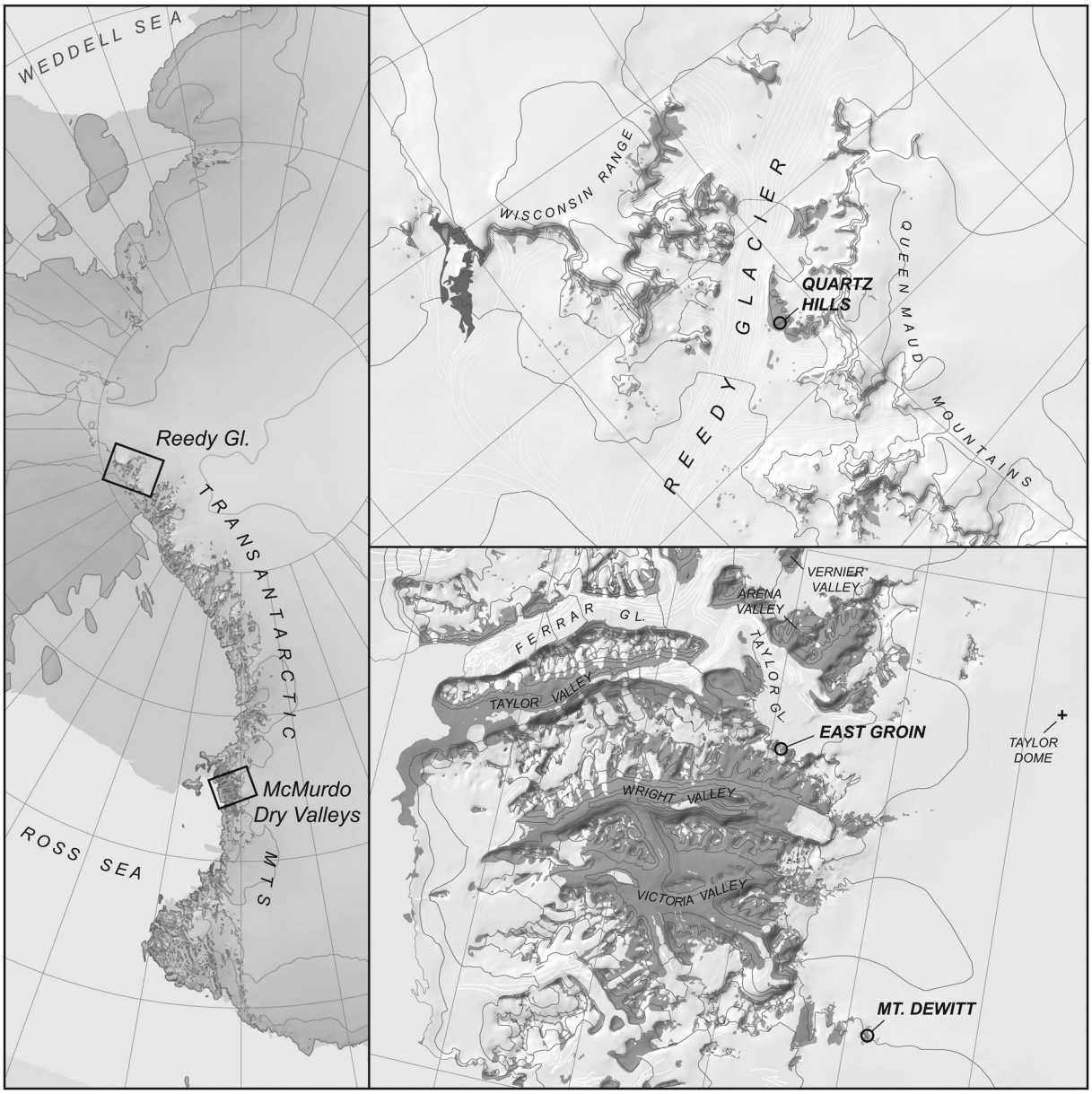

Fig. 1. Site locations. Raster data from the Antarctic Digital Database; shaded-relief topography is from the RAMP digital elevation model (Liu *et al.* 2001).

This idea is important for our purposes here because many bedrock surfaces in glaciated regions show such disequilibrium (e.g. Bierman *et al.* 1999, Sugden *et al.* 2005). Many of the measurements that showed this were originally intended to determine the time these surfaces were exposed by ice retreat during the most recent deglaciation. However, the observations that: i) nuclide concentrations were much higher (in some cases by orders of magnitude) than could have accumulated since ice retreat, and ii) ^{26}Al and ^{10}Be concentrations were not in equilibrium with continuous surface exposure, showed that these surfaces had not experienced significant subglacial erosion. Thus, cosmogenic nuclide concentrations in these surfaces record the integrated effect of not one but many periods of exposure and ice cover. These surfaces are not useful for dating the most recent ice retreat, but can potentially be used to learn about ice sheet history and surface weathering rates over many glacial-interglacial cycles.

This paper describes measurements of the cosmic ray-produced nuclides ^{26}Al ($t_{1/2}$ = 0.7 Ma), ^{10}Be ($t_{1/2}$ = 1.4 Ma) and ^{21}Ne (stable) in quartz from surfaces with geomorphic and stratigraphic evidence, as well as cosmogenic nuclide concentrations, that imply preservation under repeated

https://doi.org/10.1017/S0954102014000261 Published online by Cambridge University Press

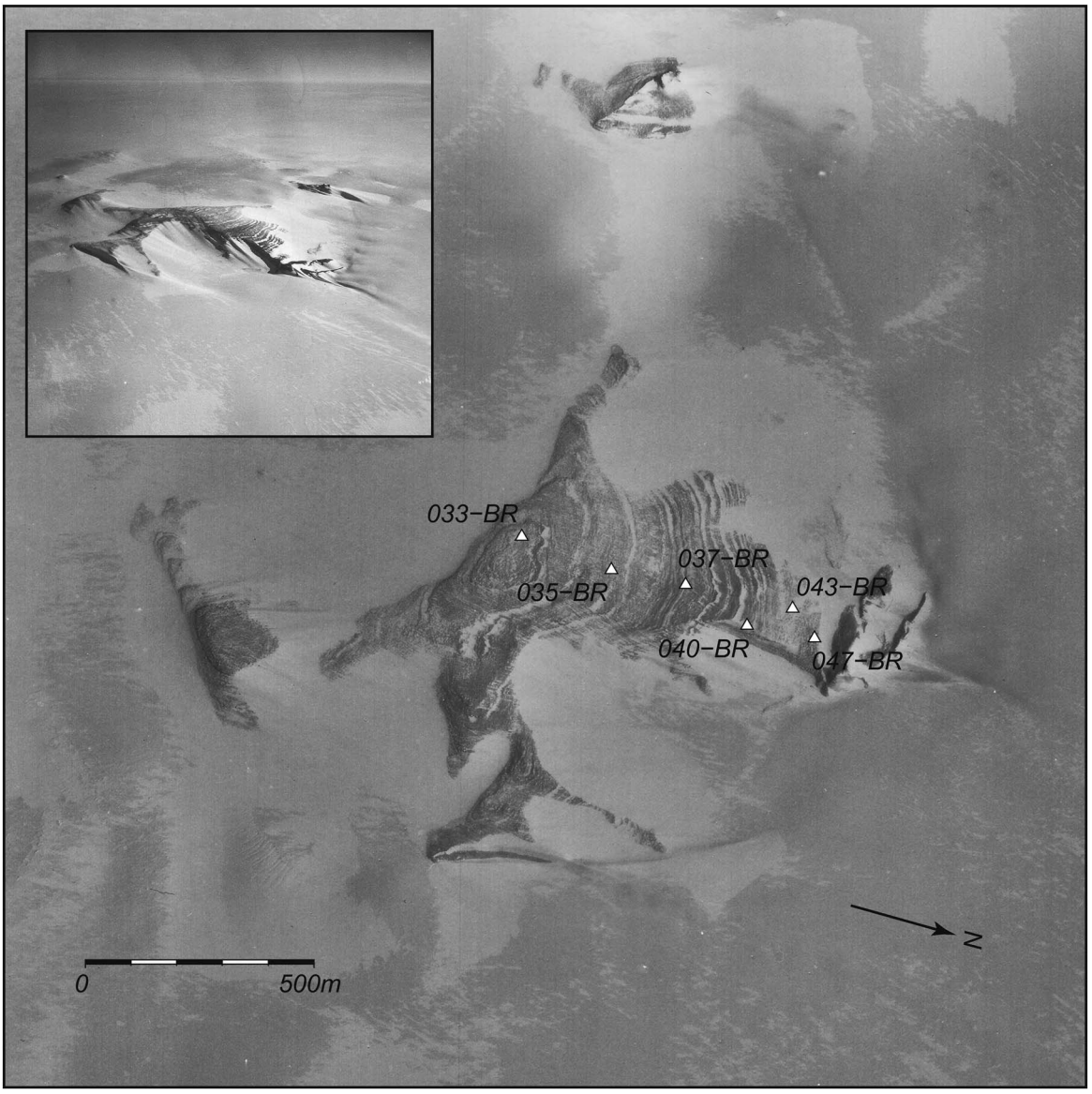

Fig. 2. Overhead (US Navy photo, line TMA2467, frame 21) and oblique (inset, line TMA279, frame 59) aerial photographs of Mount DeWitt, showing sample locations. The change in tone of the surface immediately above sample 037-BR reflects the density of dark-coloured dolerite erratics on the surface; the lower portion of the site is densely covered with erratics (e.g. Fig. 3), but the upper portion is not.

episodes of cover by frozen-based ice. All the sites have nuclide concentrations that require an exposure history extending over many glacial-interglacial cycles, and many sites show disequilibrium between concentrations of various nuclides. We explore to what extent this information can be used to learn about the history of the East Antarctic Ice Sheet over the past several million years.

Field sites

This paper describes observations from three sites (Fig. 1). Two sites, Mount DeWitt and East Groin, are located in the McMurdo Dry Valleys in Victoria Land near 77°S. The third site is located in the Quartz Hills in the southern Transantarctic Mountains near 86°S. At all three sites, stratigraphic and geomorphic observations showed that all or nearly all of the sample locations were covered by glacier ice at least once, either by expansion of the East Antarctic Ice Sheet or by advances of adjacent glaciers.

Mount DeWitt is a nunatak on the westernmost edge of the Dry Valleys, directly adjacent to the polar plateau of the East Antarctic Ice Sheet (Fig. 2). Bedrock samples were collected between 1880 m and the summit at 2090 m.

https://doi.org/10.1017/S0954102014000261 Published online by Cambridge University Press

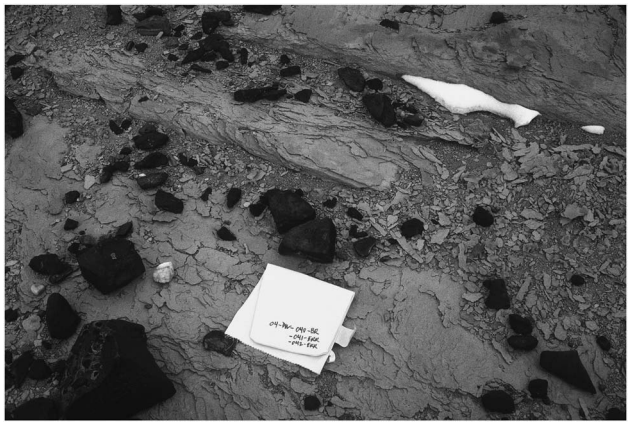

Fig. 3. Photograph of representative sample site (04-DW-040-BR, 1948 m elevation) at Mount DeWitt. Glacially transported clasts of Ferrar dolerite overlie weathered sandstone bedrock displaying weathering rinds, granular disintegration and loose surface clasts detached from the underlying bedrock.

Fig. 5. Photograph of the lowest sample site (05-EG-127-BR) at East Groin. Presumed glacial drift including clasts of Ferrar dolerite overlies sandstone that displays weathering rinds as well as loose surface clasts detached from the underlying bedrock. View is up the Taylor Glacier to the north-west.

The bedrock surface consists of weathered carbonaceous sandstone of the Triassic Lashly Formation. Clasts of Ferrar dolerite, a dark mafic intrusive rock that occurs throughout the Dry Valleys, litter the surface (Fig. 3). As this lithology does not outcrop on Mount DeWitt itself, these clasts must be glacially transported. Above 1900 m, the frequency of dolerite erratics decreases notably; erratics are sparse between 1900–2040 m. Further search above 2040 m yielded only one isolated erratic clast directly at the summit. As the summit of Mount DeWitt was occupied for extended periods by researchers maintaining positioning transponders during the Taylor Dome ice coring project, it is possible that this erratic was not naturally present at the summit. Thus, Mount DeWitt was ice-covered at some time in the past to at least 2040 m elevation, but evidence that the summit at 2090 m was ever covered is weak.

Fig. 4. Photograph of East Groin, looking SSE across the Taylor Glacier towards the Quartermain Mountains, including Arena and Beacon valleys. The site of the uppermost sample (05-EG-118-BR, 1721 m) is in the foreground. Sandstone bedrock, that displays weathering rinds and loose surface clasts detached from the underlying bedrock, is overlain by a scatter of clasts of different lithology that were probably glacially transported. Other sample sites are located along the crest of the sandstone ridge and at its toe near the glacier margin.

East Groin is a sandstone buttress adjacent to lower Taylor Glacier (Figs 4 & 5). Samples collected at this site lay between the modern ice margin at 1380 m and the highest point accessible on foot at 1720 m. The bedrock is quartz arenite sandstone of the Devonian Altar Mountain and Arena Formations. Dolerite clasts, although present at all elevations, are not necessarily diagnostic of ice cover at this site because Ferrar dolerite outcrops above our sample sites. Thus, dolerite clasts at lower elevations could conceivably have been emplaced by rockfall, although the convex form of the buttress makes it unlikely that this process would lead to the observed widespread, sparse and approximately uniform distribution of dolerite clasts. However, large quartzite cobbles derived from conglomerate facies of Beacon group sandstones, which were not observed in outcrop at this site, do indicate transport by ice. In addition, Arena Valley, directly across the Taylor Glacier from this site, contains a moraine sequence that shows that at least 500 m of thickening of Taylor Glacier took place at least once in the past several million years (Brook &

https://doi.org/10.1017/S0954102014000261 Published online by Cambridge University Press

Fig. 6. Overview of sample transect at the Quartz Hills, viewed from the medial moraine between Colorado and Reedy glaciers. The sample transect approximately follows the right-hand skyline of the prominent ridge in the middle ground. The main Quartz Hills bench of Bromley *et al.* (2010) sits left of the ridge, at mid height in the photo. Light grey deposits covering the bench and running across the base of the ridge mark the limit of Last Glacial Maximum ice cover. Darker deposits covering the ridge face, left of the exposed bedrock, are older Reedy B and Reedy D drifts (Bromley *et al.* 2010). Ice responsible for deposition of Reedy D and Reedy E drifts overtopped the bedrock spur.

Fig. 7. Location of sample 03-RDY-096-QZH (1400 m) at the bottom of the Quartz Hills elevation transect. The modern ice margin is visible in the background. The bedrock surface displays a weathering rind in places, granular disintegration and weathering pits. Glacially transported clasts in the potholes on the bedrock surface were emplaced at the Last Glacial Maximum 14–17 ka.

Kurz 1993). Thus, it is most probable that all of our sample sites were covered by expanded Taylor Glacier ice at least once in the past.

The Quartz Hills are a mountainous ice-free area adjacent to Reedy Glacier. Benches and valleys in the Quartz Hills are covered by extensive glacial deposits ranging in age from Holocene to Pliocene or older (Mercer 1968, Bromley *et al.* 2010). Granite bedrock samples were collected between 1400 m, near the present ice surface elevation, and 1675 m along a ridge overlooking the confluence of Reedy and Colorado glaciers on the west side of the 'Quartz Hills bench' (Bromley *et al.* 2010) (Figs 6, 7). The toe of the ridge is covered by Last Glacial Maximum (LGM) aged glacial drift deposited 14–17 ka (Todd *et al.* 2010), and the lowest sample (03-RDY-096-QZH; 1400 m elevation) was collected from a rock buttress projecting from this drift 10 m below its upper limit. A thin scatter of cobbles associated with the older Reedy B drift, which is believed to have been emplaced during marine isotope stage 6 at 140–160 ka (Bromley *et al.* 2010), extends to *c*. 1460 m elevation, 10 m above the second-lowest sample (03-RDY-095-QZH; 1448 m elevation). No erratics are present directly on the bedrock ridge above the Reedy B drift, but all of our samples lie below the mapped upper limit of Reedy D and E drifts on the adjacent bench (these drifts are > 3.5 Ma and > 4.5 Ma, respectively; Bromley *et al.* 2010). Thus, all of the sample sites must have been ice-covered when these drifts were emplaced.

Despite evidence for ice cover at all sites, none of the sampled bedrock surfaces show any evidence of subglacial erosion. Striations, polish, streamlining, plucking or any other features characteristic of glacial erosion are absent. In contrast, all sites show surface features characteristic of extended weathering under ice-free conditions, including weathering rinds, granular disintegration, frost-shattering, weathering pits, and fragile, cavernous forms (Figs 3, 4, 5 & 7). Thus, geomorphic observations indicate that these bedrock surfaces have been subject to slow subaerial weathering during ice-free periods, but not to subglacial erosion during periods of ice cover. As we will show later, cosmogenic nuclide concentrations are consistent with this conclusion.

Analytical methods

Physical and chemical preparation of quartz samples was carried out by the authors in the Cosmogenic Nuclide Lab at the University of Washington. This involved isolation of quartz from crushed rock samples by repeated etching in dilute hyrodfluoric acid (HF), extraction of Be and Al using standard methods of HF dissolution and column chromatography (Stone 2001), and total Al concentrations were measured by inductively coupled plasma (ICP) optical emission spectrophotometry of an aliquot of the dissolved quartz-HF solution. Be and Al isotope ratios were measured by accelerator mass spectrometry at both the Center for Accelerator Mass Spectrometry, Lawrence Livermore National Laboratory (LLNL-CAMS; Quartz Hills samples) and the Purdue Rare Isotope Measurement Laboratory (PRIME Lab;

https://doi.org/10.1017/S0954102014000261 Published online by Cambridge University Press

Table I. Site information and cosmogenic nuclide concentrations.

Sample name	Latitude (DD)	Longitude (DD)	Elevation (m)	Thickness (cm)	Density (g cm^{-2})	Topographic shielding	[^{10}Be]† (10^6 atoms g^{-1})	[^{26}Al]‡ (10^6 atoms g^{-1})	Excess [^{21}Ne]$^{\#}$ (10^6 atoms g^{-1})	Cosmogenic [^{21}Ne]§ (10^6 atoms g^{-1})	No. of ^{21}Ne analyses$^{¥}$
Mount DeWitt sandstone bedrock											
04-DW-033-BR	-77.2046	159.8414	2091	3	2.2	1.000	19.7 ± 1.2	120.5 ± 3.0	130.8 ± 4.2	123.1 ± 4.8	2
04-DW-035-BR	-77.2012	159.8422	2038	2	2.2	0.999	19.95 ± 0.79	113.1 ± 2.8	126.6 ± 3.9	118.9 ± 4.6	2
04-DW-037-BR	-77.1987	159.8415	1993	3.5	2.2	0.999	18.99 ± 0.68	106.9 ± 2.8	139.0 ± 5.1	131.3 ± 5.6	2
04-DW-040-BR	-77.1962	159.8436	1948	2.5	2.2	0.999	25.0 ± 1.0	129.5 ± 5.0	170.8 ± 6.1	163.1 ± 6.6	1
04-DW-043-BR	-77.1949	159.8410	1905	4	2.2	0.998	10.91 ± 0.31	66.7 ± 2.2	71.2 ± 2.1	63.5 ± 3.2	3
04-DW-047-BR	-77.1939	159.8430	1878	6	2.2	0.998	15.95 ± 0.37	75.4 ± 3.4	102.2 ± 3.7	94.5 ± 4.4	2
East Groin sandstone bedrock											
05-EG-118-BR	-77.6419	160.9399	1721	7	2.2	0.982	20.56 ± 0.20	101.7 ± 3.3	133.8 ± 3.2	126.1 ± 4.0	2
05-EG-119-BR	-77.6442	160.9446	1671	7	2.2	0.998	12.69 ± 0.20	66.4 ± 1.8	78.3 ± 2.4	70.6 ± 3.4	3
05-EG-120-BR	-77.6534	160.9511	1597	2.5	2.2	1.000	10.65 ± 0.19	59.1 ± 1.5	62.5 ± 3.1	54.8 ± 4.0	1
05-EG-122-BR	-77.6611	160.9420	1514	2.5	2.2	0.999	26.85 ± 0.55	113.8 ± 2.9	216.7 ± 5.5	209.0 ± 6.0	1
05-EG-123-BR	-77.6720	160.9639	1308	2.5	2.2	0.998	9.00 ± 0.15	41.4 ± 1.2	74.4 ± 3.2	66.7 ± 4.0	3
05-EG-124-BR	-77.6720	160.9639	1314	10	2.2	0.998	10.03 ± 0.15	38.5 ± 1.5	119.0 ± 8.4	111.3 ± 8.7	2
05-EG-126-BR	-77.6649	160.9468	1398	4	2.2	0.991	8.89 ± 0.13	45.2 ± 1.5	59.6 ± 2.8	51.9 ± 3.7	2
05-EG-127-BR	-77.6650	160.9392	1382	7	2.2	0.996	14.04 ± 0.18	67.1 ± 1.7	104.6 ± 4.4	96.9 ± 5.0	2
Quartz Hills bedrock											
03-RDY-090-QZH	-85.9050	-132.8025	1675	2	2.7	1.000	39.57 ± 0.40	158.5 ± 2.5	434 ± 10	426 ± 11	1
03-RDY-091-QZH	-85.9037	-132.8106	1618	2	2.7	0.959	38.90 ± 0.34	147.8 ± 2.5	399 ± 10	391 ± 10	1
03-RDY-092-QZH	-85.9032	-132.8129	1576	2	2.7	0.932	31.43 ± 0.28	127.8 ± 1.7	265.3 ± 8.2	257.6 ± 8.5	1
03-RDY-093-QZH	-85.9029	-132.8144	1549	2	2.7	0.945	36.21 ± 0.35	134.2 ± 2.0	409 ± 11	401 ± 11	1
03-RDY-094-QZH	-85.9022	-132.8194	1503	2	2.7	0.927	31.87 ± 0.28	127.1 ± 1.8	304.5 ± 8.5	296.8 ± 8.8	1
03-RDY-095-QZH	-85.9022	-132.8501	1448	2	2.7	0.945	33.32 ± 0.29	125.8 ± 1.9	331.6 ± 9.0	323.9 ± 9.4	1
03-RDY-096-QZH	-85.9003	-132.8376	1400	2	2.7	0.930	26.49 ± 0.23	103.8 ± 1.5	263.7 ± 7.0	256.0 ± 7.4	1

†Normalized to the Be isotope ratio standards of Nishiizumi *et al*. (2007), ‡normalized to the isotope ratio standards of Nishiizumi (2004), $^{\#}$ ^{21}Ne not accounted for by trapped Ne of atmospheric composition. Includes both cosmogenic and nucleogenic ^{21}Ne; §reflects subtraction of estimated nucleogenic ^{21}Ne reflects concentration from measured excess ^{21}Ne concentration. $^{¥}$Complete results of step-degassing Ne analyses appear in a supplemental table.

Table II. Apparent exposure ages and erosion rates inferred from ^{26}Al, ^{10}Be and ^{21}Ne concentrations individually.

	Apparent exposure ages (Ma)									Apparent erosion rates (m Ma^{-1})								
Sample name	From ^{10}Be	Internal uncertainty	External uncertainty	From ^{26}Al	Internal uncertainty	External uncertainty	From ^{21}Ne	Internal uncertainty	External uncertainty	From ^{10}Be	Internal uncertainty	External uncertainty	From ^{26}Al	Internal uncertainty	External uncertainty	From ^{21}Ne	Internal uncertainty	External uncertainty
Mount DeWitt bedrock																		
04-DW-033-BR	0.68	0.05	0.09	0.73	0.03	0.10	0.88	0.03	0.09	0.92	0.08	0.14	0.70	0.04	0.13	0.90	0.04	0.08
04-DW-035-BR	0.72	0.03	0.08	0.70	0.03	0.09	0.88	0.03	0.09	0.86	0.05	0.12	0.74	0.04	0.13	0.90	0.04	0.08
04-DW-037-BR	0.71	0.03	0.08	0.68	0.03	0.09	1.01	0.04	0.11	0.87	0.05	0.12	0.76	0.04	0.13	0.79	0.03	0.07
04-DW-040-BR	1.04	0.06	0.13	0.95	0.06	0.15	1.29	0.05	0.14	0.54	0.04	0.09	0.47	0.05	0.11	0.62	0.03	0.05
04-DW-043-BR	0.41	0.01	0.04	0.40	0.02	0.05	0.52	0.03	0.06	1.66	0.06	0.18	1.52	0.07	0.21	1.53	0.08	0.14
04-DW-047-BR	0.65	0.02	0.07	0.49	0.03	0.06	0.81	0.04	0.09	0.96	0.03	0.12	1.19	0.09	0.19	1.00	0.05	0.09
East Groin bedrock																		
05-EG-118-BR	1.07	0.01	0.12	0.91	0.05	0.14	1.24	0.04	0.13	0.52	0.01	0.08	0.51	0.04	0.11	0.66	0.02	0.05
05-EG-119-BR	0.60	0.01	0.06	0.51	0.02	0.06	0.71	0.03	0.08	1.06	0.02	0.12	1.13	0.05	0.17	1.15	0.06	0.10
05-EG-120-BR	0.51	0.01	0.05	0.45	0.01	0.05	0.56	0.04	0.07	1.30	0.03	0.15	1.31	0.05	0.18	1.45	0.11	0.15
05-EG-122-BR	1.86	0.06	0.28	1.37	0.07	0.26	2.29	0.07	0.24	0.24	0.01	0.05	0.26	0.03	0.09	0.36	0.01	0.03
05-EG-123-BR	0.54	0.01	0.06	0.39	0.01	0.04	0.86	0.05	0.10	1.21	0.03	0.14	1.60	0.07	0.21	0.97	0.06	0.09
05-EG-124-BR	0.65	0.01	0.07	0.38	0.02	0.04	1.51	0.12	0.19	0.98	0.02	0.12	1.67	0.09	0.22	0.56	0.04	0.06
05-EG-126-BR	0.50	0.01	0.05	0.40	0.02	0.05	0.63	0.04	0.08	1.32	0.03	0.15	1.53	0.07	0.21	1.31	0.10	0.14
05-EG-127-BR	0.90	0.01	0.10	0.70	0.03	0.09	1.22	0.06	0.14	0.66	0.01	0.09	0.74	0.04	0.13	0.69	0.04	0.06
Quartz Hills bedrock																		
03-RDY-090-QZH	3.12	0.08	0.67	2.43	0.16	0.89	4.12	0.10	0.42	0.080	0.005	0.030	0.060	0.010	0.060	0.161	0.004	0.013
03-RDY-091-QZH	3.74	0.10	0.98	2.59	0.20	1.05	4.12	0.11	0.43	0.050	0.005	0.030	0.050	0.010	0.060	0.162	0.004	0.013
03-RDY-092-QZH	2.58	0.05	0.47	1.91	0.07	0.49	2.88	0.10	0.30	0.110	0.007	0.040	0.110	0.010	0.060	0.234	0.008	0.019
03-RDY-093-QZH	3.71	0.11	0.96	2.30	0.13	0.77	4.52	0.12	0.47	0.050	0.005	0.030	0.070	0.010	0.060	0.149	0.004	0.012
03-RDY-094-QZH	3.05	0.06	0.64	2.30	0.13	0.77	3.53	0.10	0.37	0.080	0.005	0.030	0.070	0.010	0.060	0.192	0.006	0.015
03-RDY-095-QZH	3.67	0.09	0.94	2.43	0.15	0.89	3.95	0.11	0.41	0.060	0.005	0.030	0.060	0.010	0.060	0.172	0.005	0.014
03-RDY-096-QZH	2.43	0.04	0.42	1.60	0.06	0.34	3.30	0.09	0.34	0.130	0.007	0.040	0.160	0.010	0.060	0.208	0.006	0.017

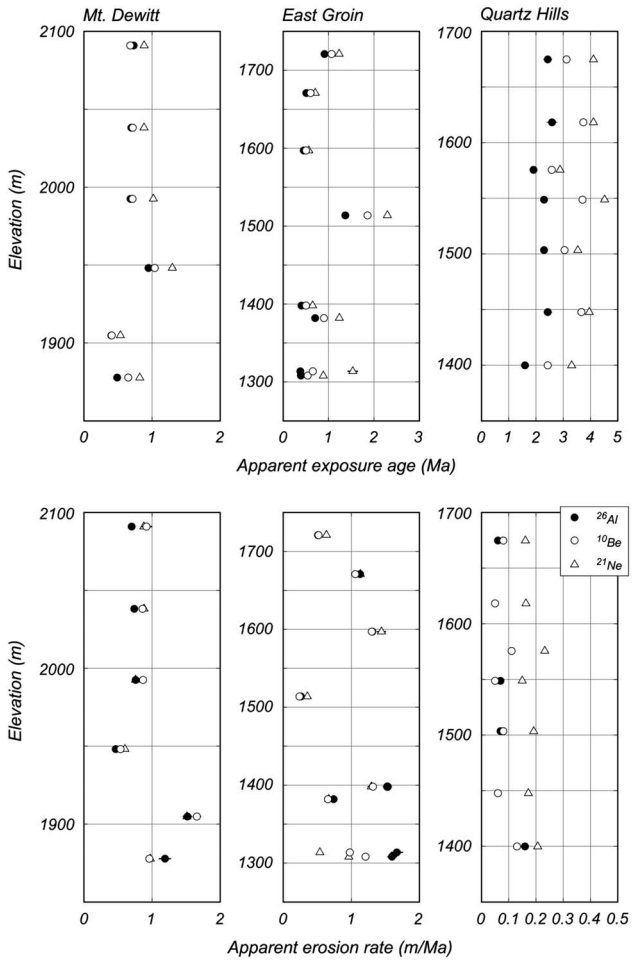

Fig. 8. Apparent exposure age–elevation and apparent erosion rate–elevation relationships at Mount DeWitt, East Groin, and the Quartz Hills. Error bars (1σ) reflect measurement uncertainty (where not visible error bars are smaller than the size of the symbols).

Mount DeWitt and East Groin samples). The ^{26}Al and ^{10}Be concentrations are shown in Table I. The ^{9}Be carrier was a commercially available Be ICP standard solution. For samples measured at PRIME, full carrier and process blanks had 277 000 ± 77 000 atoms ^{10}Be, in all cases < 0.5% of the total number of ^{10}Be atoms in the sample, and 230 000 ± 93 000 atoms ^{26}Al, in all cases < 0.2% of the total number of atoms in the sample. For samples measured at LLNL-CAMS, full carrier and process blanks had 66 000 ± 28 000 atoms ^{10}Be, in all cases < 0.3% of the total number of atoms in the sample, and 65 000 ± 40 000 atoms ^{26}Al, in all cases < 0.2% of the total number of atoms in the sample.

Ne was extracted from aliquots of the same HF-etched quartz samples in the Noble Gas Thermochronometry Lab of the Berkeley Geochronology Center by encapsulating the sample in a Ta packet and heating it under vacuum with a 75 W, 810 nm diode laser. The released Ne was analysed on a MAP-215 mass spectrometer using a method that employs an ^{39}Ar spike to correct for isobaric interferences on masses 20 and 22 (Balco & Shuster 2009a). The Ne isotope ratios in all heating steps were consistent with two-component mixing between atmospheric and cosmogenic Ne, i.e. they were not distinguishable at 95% confidence from the atmospheric-cosmogenic mixing line (Niedermann *et al.* 1993). However, quartz from Beacon Group sandstones in the Dry Valleys is known to contain nucleogenic ^{21}Ne produced by the reaction ^{18}O(α,n)^{21}Ne as a result of uranium and thorium decay. Both Middleton *et al.* (2012) and Balco *et al.* (2011) found, at different sites, that quartz in Beacon Group sandstones contained 7.7×10^6 atoms g^{-1} nucleogenic ^{21}Ne. Given the high total ^{21}Ne concentrations and characteristic measurement precision for the samples in this study, this amount of nucleogenic ^{21}Ne is not sufficient to recognizably displace measured Ne isotope ratios from the atmospheric-cosmogenic mixing line. Thus, we calculated cosmogenic ^{21}Ne concentrations by i) first computing excess ^{21}Ne relative to atmospheric composition, and then ii) subtracting $7.7 \pm 2.4 \times 10^6$ atoms g^{-1} from this amount (the uncertainty estimate for the nucleogenic ^{21}Ne concentration is from Middleton *et al.* (2012)). The samples from the Quartz Hills are not Beacon Group sandstones; therefore, this is probably not an accurate estimate of the nucleogenic ^{21}Ne concentration in these samples. However, this amount of nucleogenic ^{21}Ne would be at most 2.5% of the total excess ^{21}Ne concentration in any sample from the Quartz Hills. Thus, we accept even a large uncertainty in our estimate of nucleogenic ^{21}Ne for these samples as negligible relative to measurement uncertainty. Summary ^{21}Ne concentrations are presented in Table I and complete results of the step-degassing analyses are shown in Table S1 (found at http://dx.doi.org/10.1017/S0954102014000261).

Production rates and decay constants

Production rates for ^{10}Be due to spallation were computed using the global calibration dataset and 'St' scaling scheme of Balco *et al.* (2008), the assumed spallogenic production ratios ^{26}Al/^{10}Be, ^{21}Ne/^{10}Be and ^{21}Ne/^{26}Al were 6.75, 4.08 and 0.61, respectively (Balco & Shuster 2009a). The decay constants for ^{26}Al and ^{10}Be used were 9.83 x 10^{-7} and 4.99 x 10^{-7}, respectively (Nishiizumi 2004, Chmeleff *et al.* 2009, Korschinek *et al.* 2010). Balco & Shuster (2009b) showed that this set of production ratios and decay constants, if not yet incontrovertibly correct, are at least internally consistent. Note that our conclusions rely primarily on these estimates of production ratios and decay constants, and are very weakly dependent on the actual magnitude of production rates. Thus, recent work (e.g. Balco *et al.* 2009) showing that the actual ^{10}Be production rates predicted by the global

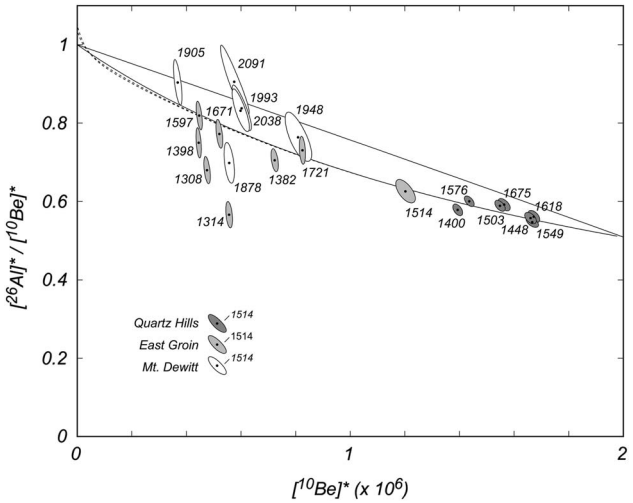

Fig. 9. ^{26}Al-^{10}Be two-nuclide diagram. See Granger (2006) for a complete discussion of this diagram. *Nuclide concentrations normalized to respective surface production rates. Solid black lines = 'simple exposure region', the region of the diagram where nuclide concentrations can lie given a single period of continuous surface exposure at any erosion rate. Upper boundary = 'simple exposure line', nuclide concentrations permissible given continuous surface exposure and zero erosion. Lower boundary = 'steady erosion line', nuclide concentrations expected if a surface has eroded steadily for long enough to reach equilibrium. Nuclide concentrations that lie between the boundary lines are in equilibrium with continuous surface exposure. Solid boundary lines reflect spallogenic production only. Dashed lines include production by muons, showing that the effect of muon production is negligible compared to measurement uncertainty for samples with high apparent exposure ages; The contribution of muons to total production varies with elevation, two lines are drawn to span the range of sample elevations. Ellipses are 68% confidence regions reflecting measurement uncertainties only. Datapoint labels are sample elevations.

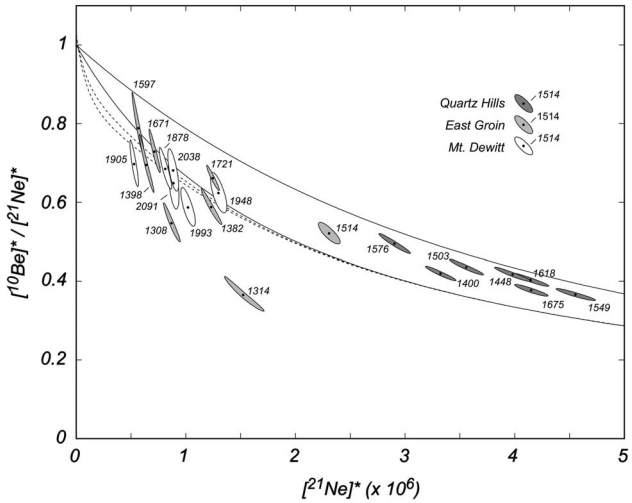

Fig. 10. ^{10}Be-^{21}Ne two-nuclide diagram (see Fig. 9 for description of diagram construction and symbols).

calibration dataset of Balco *et al.* (2008) are probably inaccurate at the *c.* 5–10% level has a negligible effect on our conclusions. The ^{26}Al and ^{10}Be production by muons was computed using the method of Heisinger *et al.* (2002b, 2002a) as implemented in Balco *et al.* (2008). Production of ^{21}Ne by muons has not been directly measured. However, Balco *et al.* (unpublished) found that cosmogenic ^{21}Ne concentrations in a deep sandstone core were consistent with muon interaction cross-sections estimated by Fernandez-Mosquera *et al.* (2010). Thus, these cross-sections were adopted. It is important to note that because the samples in this study have very high concentrations of spallogenic ^{26}Al, ^{10}Be, and ^{21}Ne, concentrations of these nuclides due to muon production are small by comparison, and even large uncertainties in estimating production rates due to muons have a negligible effect on any of our conclusions.

Results

Measured ^{26}Al, ^{10}Be and ^{21}Ne concentrations appear in Table I.

Discussion

Table II and Fig. 8 represent nuclide concentrations as apparent exposure ages or as apparent erosion rates. An 'apparent exposure age' is the exposure age calculated assuming a single period of continuous exposure at zero erosion, and an 'apparent erosion rate' is the surface erosion rate implied by the nuclide concentration given the assumption of continuous steady erosion for

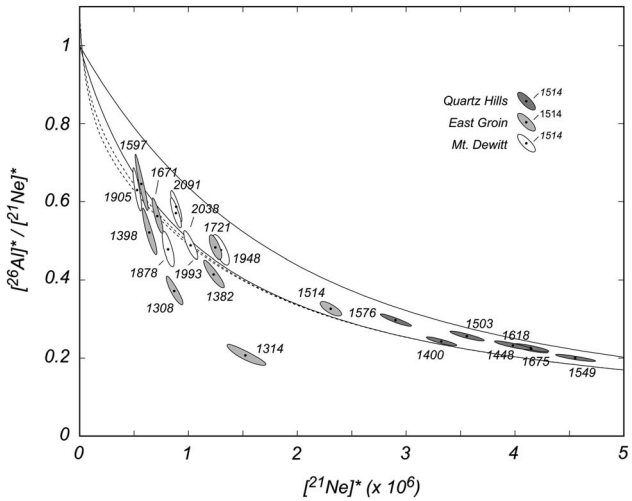

Fig. 11. ^{26}Al-^{21}Ne two-nuclide diagram (see Fig. 9 for description of diagram construction and symbols).

https://doi.org/10.1017/S0954102014000261 Published online by Cambridge University Press

long enough that nuclide concentrations have reached equilibrium between production and loss by surface erosion and radioactive decay. In addition, Figs 9, 10 & 11 show normalized two-nuclide diagrams for the three nuclide pairs ^{26}Al-^{10}Be, ^{21}Ne-^{10}Be and ^{21}Ne-^{26}Al.

Key features of the data

High elevation samples at Dry Valleys sites are consistent with steady surface erosion and production-decay-erosion equilibrium. At higher elevation sites at both Mount DeWitt (above 1900 m) and East Groin (above 1400 m), apparent exposure ages vary between different nuclides, but apparent erosion rates are indistinguishable (Fig. 8). In other words, concentrations of all three nuclides in these samples are not consistent with the hypothesis that these surfaces have experienced a single period of exposure at zero erosion, but they are consistent with the hypothesis that the surfaces have been eroding steadily for a long enough time that nuclide concentrations have reached an equilibrium between production and loss by radioactive decay and surface erosion. As evident from Figs 9, 10 & 11, this is equivalent to observing that these samples lie on the steady erosion line with respect to all three nuclide pairs. Thus, the simplest explanation for these results is that these surfaces have been experiencing steady erosion at 0.5–1.5 m Ma^{-1} for a long time. How long a period of steady erosion is implied? The rate at which surface nuclide concentrations approach equilibrium with steady erosion depends on both the erosion rate and the decay constant of the nuclide in question. An effective half-life for equilibration with steady erosion is given by -1n (1/2)/(λ_i + ε/Λ), where λ_i is the decay constant for nuclide i (a^{-1}), ε is the erosion rate (g cm^{-2} a^{-1}), and Λ is the effective attenuation length for spallogenic production (here taken to be 160 g cm^{-2}). These effective half-lives are 0.2–1 Ma for this range of erosion rates and nuclides, thus 1–4 Ma would be required to reach 95% of the equilibrium value. Therefore, there is no evidence that any of these sites were covered by ice during the past 1–4 Ma. The strength of this constraint is discussed later.

Low elevation samples at Dry Valleys sites require periods of ice cover. Low elevation sites at Mount DeWitt (one site at 1878 m) and East Groin (four sites between 1314–1382 m) show neither apparent exposure ages nor apparent erosion rates that are concordant between nuclides (Fig. 8). In other words, nuclide concentrations are neither consistent with continuous surface exposure at zero erosion nor with steady erosion. These samples lie outside the continuous exposure field on all three two-nuclide diagrams, in the region of intermittent exposure (Figs 9, 10 & 11). Thus, these sites have experienced at least one period of ice cover during their exposure history.

High elevation samples at the Quartz Hills display production-erosion equilibrium for ^{26}Al and ^{10}Be, but not for ^{21}Ne. At all sites in the Quartz Hills, apparent exposure ages differ significantly between all three nuclides, indicating that these sites have not experienced continuous surface exposure at zero erosion. However, apparent erosion rates derived from ^{26}Al and ^{10}Be are i) indistinguishable from each other and ii) significantly different from the apparent ^{21}Ne erosion rate. This is most simply explained if these surfaces have been continuously exposed and subject to steady erosion for a sufficient length of time that ^{26}Al and ^{10}Be concentrations have reached equilibrium with steady erosion, but ^{21}Ne concentrations have not. This is also evident on the two-nuclide diagrams: nuclide concentrations in these samples lie on the steady erosion line in the ^{26}Al-^{10}Be diagram, but lie between the simple exposure and steady erosion lines in ^{26}Al-^{21}Ne and ^{10}Be-^{21}Ne diagrams. At the erosion rates implied by the ^{26}Al and ^{10}Be concentrations (*c*. 0.1 m Ma^{-1}) the effective half-lives for ^{26}Al and ^{10}Be equilibration with steady erosion are 0.6 Ma and 1 Ma, respectively. Therefore, 3–4 Ma is required for ^{26}Al and ^{10}Be concentrations to become indistinguishable from erosional steady state. However, erosion rates of these surfaces are low enough that a significant fraction of loss of ^{26}Al and ^{10}Be from the surface is the result of radioactive decay, not erosion. Since ^{21}Ne is stable, it can only be lost by erosion, thus the effective half-life for ^{21}Ne equilibration with steady erosion at the erosion rate implied by the ^{26}Al and ^{10}Be concentrations is 4 Ma, much longer than for ^{26}Al or ^{10}Be. Thus, *c*. 15–20 Ma would be required before ^{21}Ne concentrations were indistinguishable from production-erosion equilibrium. In other words, the ^{21}Ne concentrations retain a memory of the time these sites were first exposed, but ^{26}Al and ^{10}Be concentrations do not. If we assume a single period of continuous surface exposure at a steady erosion rate, with negligible production by muons, we can estimate both the exposure age and erosion rate of these samples by solving the (overdetermined) system of equations:

$$N_{26} = \frac{P_{26}}{\lambda_{26} + \frac{\varepsilon}{\Lambda}}\left(1 - \exp\left[-\left(\lambda_{26} + \frac{\varepsilon}{\Lambda}\right)t\right]\right) \quad (1)$$

$$N_{10} = \frac{P_{10}}{\lambda_{10} + \frac{\varepsilon}{\Lambda}}\left(1 - \exp\left[-\left(\lambda_{10} + \frac{\varepsilon}{\Lambda}\right)t\right]\right) \quad (2)$$

$$N_{21} = \frac{P_{26}\Lambda}{\varepsilon}\left(1 - \exp\left[-\left(\frac{\varepsilon}{\Lambda}\right)t\right]\right) \quad (3)$$

for the erosion rate ε (g cm^{-2} a^{-1}) and the exposure time t (a), where N_i is the concentration (atoms g^{-1}) and P_i is the surface production rate (atoms g^{-1} a^{-1}) of nuclide i. Because, as described above, stratigraphic and geomorphic evidence shows that these sites were covered by ice at least

https://doi.org/10.1017/S0954102014000261 Published online by Cambridge University Press

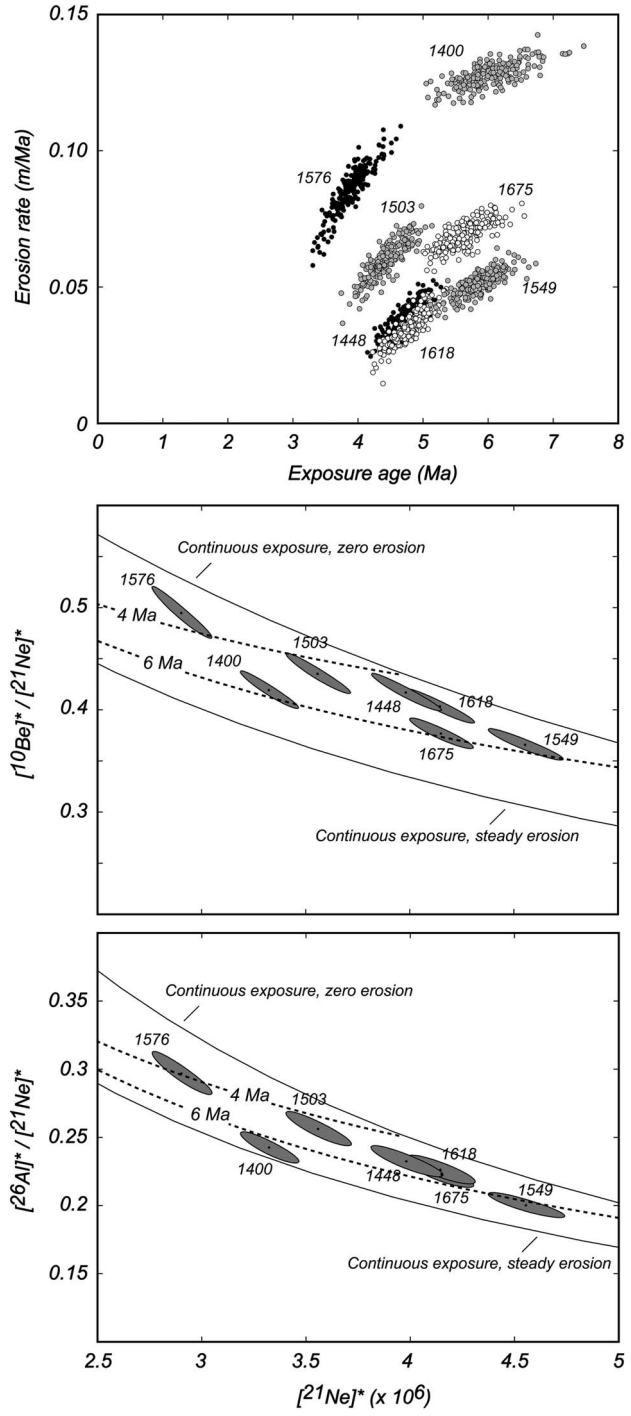

Fig. 12. Upper panel, exposure ages and erosion rates calculated by solving the system of Eqs (1)–(3) for samples at the Quartz Hills. The dots are the result of a 200-point Monte Carlo simulation including measurement uncertainty only. The middle and lower panels show sections of ^{26}Al-^{21}Ne and ^{10}Be-^{21}Ne two-nuclide diagrams from Figs 10 & 11, respectively, with isolines for 4 and 6 Ma exposure duration (at a range of erosion rates) added to the continuous exposure region. This provides similar information as the upper panel by showing that all the data are consistent within measurement uncertainty with this range of exposure ages.

once, these assumptions imply that the duration of ice cover was short relative to the total duration of exposure.

The system of equations was solved for each sample using the non-linear least squares algorithm in MATLAB, and uncertainties estimated via a 200-iteration Monte Carlo simulation (Fig. 12). The results indicate that nuclide concentrations at all sites can be explained if these surfaces were originally exposed between 4–6 Ma (with nominal 68% confidence bounds on each age estimate of ± 0.25–0.4 Ma; see Fig. 12), and have been eroding at 3–12 cm Ma^{-1} since that time (given rock density of 2.7 g cm^{-3}). Surface exposure ages computed in this way are consistent with apparent exposure ages > 4 Ma on boulders from Reedy E drift (Bromley *et al.* 2010), and thus with a scenario in which initial exposure of bedrock surfaces at this site was coincident with emplacement of the Reedy E drift.

The Monte Carlo uncertainty analysis shows that exposure ages estimated in this way scatter more than expected from measurement uncertainty alone ($\chi^2 = 48$ for 6 degrees of freedom). This is probably due to two factors: first, the assumption of continuous exposure at a steady erosion rate is an oversimplification; a time-varying erosion rate or periods of cover by till could cause this assumption to fail. Second, we have disregarded stratigraphic evidence showing that these sites were, in fact, covered by ice for at least a short time. As noted by Mukhopadhyay *et al.* (2012) and others, one can easily construct exposure histories that include short periods of ice cover but yield nuclide concentrations that could be the result of continuous surface exposure. However, the fact that ice cover is not required to explain the observed nuclide concentrations shows that the duration of ice cover at these sites was short relative to their total exposure history. 'Short' in this context means thousands to tens of thousands of years; order 1–2% of the total exposure history. Furthermore, because of the geometric requirement that if higher elevation sites are covered by ice then lower elevation sites must also be covered, the fact that there is no relationship between site elevation and exposure age or erosion rate computed in this way is not consistent with a significant duration of ice cover as a source for the scatter in inferred exposure ages. To summarize, despite geomorphic evidence that all sites were covered by ice at least once in the past, the simplest explanation for the observed nuclide concentrations is that these surfaces were first exposed 4–6 Ma and have been eroding at 3–10 cm Ma^{-1} since that time, with periods of ice cover restricted to a total duration of thousands to tens of thousands of years.

Finally, it is worth noting that these are extraordinarily low erosion rates by global standards. In fact, disregarding ice cover in estimating exposure ages and erosion rates from Eqs (1)–(3) leads to overestimation of erosion rates, thus these are maximum limiting erosion rates under any assumptions.

https://doi.org/10.1017/S0954102014000261 Published online by Cambridge University Press

Constraints on ice cover history

Samples that display nuclide concentrations that are not in equilibrium with continuous surface exposure at any erosion rate must have been covered by ice for a significant fraction of their history. On the other hand, nuclide concentrations that are consistent with simple exposure do not completely exclude any ice cover of the site in the past. If episodes of ice cover were short relative to the total exposure history or if ice cover took place long enough ago that the majority of the present nuclide inventory was produced after ice cover ended, then nuclide concentrations would not be perturbed enough to be detectable. Our dataset must reflect one or both of these situations, because many samples are from sites where geological evidence requires ice cover at some time in the past, but have nuclide concentrations consistent with continuous surface exposure. This includes samples from between 1920 and 2040 m elevation at Mount DeWitt, all samples from the Quartz Hills, and samples from above 1400 m at East Groin. For one thing, this is important because it highlights the fact that nuclide concentrations that show consistency with continuous surface exposure cannot be used to prove that sample sites were never covered by ice. A few thousand years of ice cover at the LGM, for example, would not detectably perturb ^{26}Al and ^{10}Be concentrations in bedrock surfaces that already had a long exposure history. To explore this issue further we have to address two questions: first, for the samples that have ^{26}Al, ^{10}Be and ^{21}Ne concentrations consistent with simple exposure but geological evidence for ice cover, what limits can be placed on the timing and duration of past ice cover? Second, for the samples that have nuclide concentrations requiring significant ice cover, what sort of ice cover histories are consistent with the nuclide concentrations? As discussed by Bierman *et al.* (1999) and many others subsequently, these questions do not have unique answers. As the nuclide concentrations reflect the total integrated exposure and burial of the surfaces, many ice cover histories that differ in the number, duration and time of burial and exposure periods can yield the same nuclide concentrations. Thus, we will use the approach of proposing simple scenarios of ice sheet change and exploring under what conditions they are compatible with the observed nuclide concentrations.

Samples from between 1920 and 2040 m elevation at Mount DeWitt, all samples from the Quartz Hills and samples from above 1400 m at East Groin have nuclide concentrations that can be explained by continuous surface exposure. However, geological evidence shows that these sites were covered by ice at some point. Therefore, how long could these sites have been covered by ice without causing nuclide concentrations to be detectably out of equilibrium with continuous surface exposure? Because radioactive decay and surface erosion tend to efface evidence of past ice cover, the longer ago the period of burial, the longer the duration of burial can be and still satisfy this condition.

To explore this question, we will assume the following. First, the rock surface at a sample site has been steadily eroding at an erosion rate ε (g cm^{-2} a^{-1}) for a sufficient time for the nuclide concentrations to reach production-decay-erosion equilibrium. At this point, nuclide concentrations are as follows:

$$N_{26,eq} = \frac{P_{26}}{\lambda_{26} + \frac{\varepsilon}{\Lambda}} \tag{4}$$

$$N_{10,eq} = \frac{P_{10}}{\lambda_{10} + \frac{\varepsilon}{\Lambda}} \tag{5}$$

$$N_{21,eq} = \frac{P_{21,sp}\Lambda}{\varepsilon} + \frac{P_{21,\mu-}\Lambda_{\mu-}}{\varepsilon} + \frac{P_{21,\mu fast}\Lambda_{\mu fast}}{\varepsilon}. \tag{6}$$

Although we consider only spallogenic production for ^{26}Al and ^{10}Be, we separately consider production by muons for ^{21}Ne. This is because at low erosion rates, muon-produced ^{10}Be and ^{26}Al produced at depth is mostly lost to radioactive decay by the time it gets to the surface, thus ^{26}Al and ^{10}Be produced by muons is negligible by comparison with that due to spallation. This is not necessarily the case for a stable nuclide (see Balco & Shuster 2009a). Thus, $P_{21,sp}$, $P_{21,\mu-}$, and $P_{21,\mu fast}$ are surface production rates (atoms g^{-1} yr^{-1}) of ^{21}Ne by spallation, negative muon capture and fast muon interactions, respectively. For this purpose we approximate the depth dependence of muon production by a simple exponential relationship and define $\Lambda_{\mu-}$ (1510 g cm^{-2}) and $\Lambda_{\mu fast}$ (4360 g cm^{-2}) to be effective attenuation lengths for negative muon capture and fast muon interactions (Heisinger *et al.* 2002a, 2002b). The sample is covered by ice at a time t_0 (years before present) and remains covered for a duration t_b (years) (see Fig. 13). It is then exposed again and continues to erode at a rate ε until the present time. With these conditions the nuclide concentrations observed at the present time are:

$$N_{26} = N_{26,eq}\exp\left[-\lambda_{26}t_0 + \frac{-\varepsilon(t_0 - t_b)}{\Lambda}\right] + \frac{P_{26}}{\lambda_{26} + \frac{\varepsilon}{\Lambda}}\left[1 - \exp\left(-\left[\lambda_{26} + \frac{\varepsilon}{\Lambda}\right][t_0 - t_b]\right)\right] \tag{7}$$

$$N_{10} = N_{10,eq}\exp\left[-\lambda_{10}t_0 + \frac{-\varepsilon(t_0 - t_b)}{\Lambda}\right] + \frac{P_{10}}{\lambda_{10} + \frac{\varepsilon}{\Lambda}}\left[1 - \exp\left(-\left[\lambda_{10} + \frac{\varepsilon}{\Lambda}\right][t_0 - t_b]\right)\right] \tag{8}$$

$$N_{21} = N_{21,eq} \tag{9}$$

Given typical measurement precision for these nuclides of 3%, we now assume that disequilibrium with continuous

https://doi.org/10.1017/S0954102014000261 Published online by Cambridge University Press

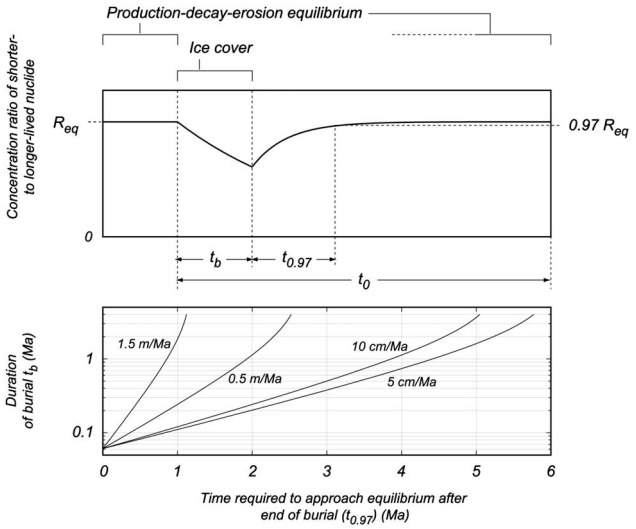

Fig. 13. An attempt to answer the question, 'if a nuclide pair displays equilibrium with steady erosion at present, what constraint does that observation place on the timing and duration of past periods of ice cover?' The upper panel shows the scenario envisioned in Eqs (4)–(9): the ratio of two nuclides (shown as the ratio of the shorter- to longer-lived nuclide) begins at a value in equilibrium with steady erosion. When the sample is buried and erosion ceases, the ratio diverges from the equilibrium ratio due to radioactive decay. When it is uncovered again and erosion resumes, the ratio recovers to the equilibrium ratio at a rate that depends on the erosion rate and the half-lives of the nuclides. The length of time ($t_{0.97}$) is how long it takes to return to 97% of the equilibrium ratio, assumed to be indistinguishable from the equilibrium ratio given typical measurement uncertainties. Thus, at time $t_{0.97}$, the period of burial would cease to be detectable. The lower panel shows the constraints implied by this scenario on the timing and duration of burial of a sample that is observed to have a ^{10}Be/^{21}Ne ratio indistinguishable from the equilibrium ratio for a given erosion rate. For example, a sample exhibiting ^{10}Be-^{21}Ne concentrations in equilibrium with 0.5 m Ma^{-1} erosion means that a period of ice cover ending 2 Ma can have been no longer than 1 Ma. When erosion rates are relatively high (1.5 m Ma^{-1}) constraints on past ice cover are relatively weak: for example, it only takes *c*. 1 Ma for the ^{10}Be-^{21}Ne system to forget about any duration of past burial. Sites with lower erosion rates provide stronger constraints.

surface exposure would be detectable if the observed ratio of two nuclides was 3% lower than the equilibrium ratio. For a particular value of ε, we ask what combinations of t_0 and t_b would satisfy this condition, i.e. be detectable at the present time? For the ^{10}Be-^{21}Ne nuclide pair, for example, this is the same as specifying a value of ε and finding the set of (t_0,t_b) pairs that satisfy $N_{10}N_{21,eq}/N_{10,eq}N_{21} = 0.97$. This nuclide pair is the slowest to return to its production-decay-erosion equilibrium after a period of burial; therefore, it gives the strongest constraints on the duration of past periods of ice cover.

The results of this exercise are shown in Fig. 13. It is important to note that a minimum of 60 000 years of continuous ice cover is required for the ^{10}Be/^{21}Ne ratio to decrease by 3% from the initial equilibrium ratio (the corresponding figures for ^{26}Al/^{10}Be and ^{26}Al/^{21}Ne are 60 000 and 30 000 years, respectively). Thus, a single period of ice cover shorter than this value would not be detectable under this criterion. Again, this highlights that nuclide concentrations that are not measurably out of equilibrium with continuous exposure may not be used to prove that a rock surface has never been covered by ice. Further, these results show that when the erosion rate is relatively high, e.g. 1 m Ma^{-1}, the observation of two-nuclide equilibrium is not very restrictive; only a relatively short time is required for nuclide concentrations to return to near-equilibrium values. For example, samples at higher elevations at Mount DeWitt and East Groin, where concentrations of all three nuclides are in equilibrium with steady erosion, indicate surface erosion rates of 0.5–1.5 m Ma^{-1}. At these erosion rates, the observation of equilibrium nuclide concentrations can exclude long periods of ice cover only in the past 1–2 Ma (Fig. 13). Even very long episodes of glacier thickening prior to that time would not be detectable. At the Quartz Hills, as discussed in the previous section, higher nuclide concentrations probably imply lower erosion rates of 5–10 cm Ma^{-1}. Because erosion rates are lower, these sites can potentially record disequilibrium induced by long periods of ice cover for a much longer time; an episode of ice cover sustained for *c*. 0.1 Ma could potentially be detectable after *c*. 1 Ma. Thus, the Quartz Hills sites provide strong evidence that, despite clear geological evidence for occasional thickening of Reedy Glacier, these episodes were rare and short-lived during the Pleistocene.

Low elevation samples at East Groin and Mount DeWitt have nuclide concentrations that cannot be explained by continuous surface exposure and thus require episodes of ice cover. These samples have probably experienced numerous periods of alternating surface exposure and burial beneath cold-based ice, such that the total duration of ice cover makes up a significant fraction of their total exposure history. For the East Groin sample sites, this is implied by moraines and glacial drift at many nearby sites adjacent to the Taylor Glacier that record glacier thickening and thinning, probably on a 100 000-year glacial-interglacial cycle (e.g. Brook & Kurz 1993, Higgins *et al.* 2000). Presumably, such cyclical glacier changes occurred during much of the Pleistocene and perhaps Pliocene. A straightforward way to evaluate whether a scenario of periodic, glacial-interglacial ice sheet change is consistent with our measurements is to hypothesize that surface nuclide concentrations have reached a dynamic steady state such that nuclide

https://doi.org/10.1017/S0954102014000261 Published online by Cambridge University Press

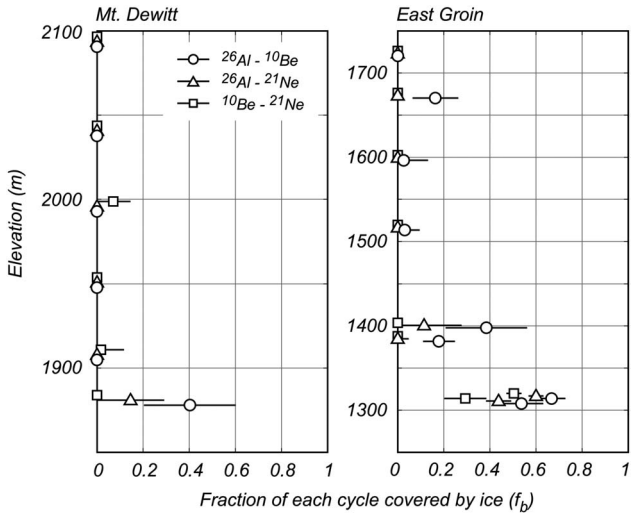

Fig. 14. Variation with elevation of the fraction f_b of each glacial cycle during which each sample site is covered by ice inferred by solving the relevant pairs of Eqs (4)–(6), for sites at Mount DeWitt and East Groin. The results from different nuclide pairs from the same sample have been slightly displaced vertically to improve readability. The error bars reflect 68% confidence intervals given measurement uncertainty only and are estimated by numerical partial differentiation and adding in quadrature. Where ice cover is never permitted by a particular nuclide pair for a particular sample no error bar is shown.

production during ice-free periods is balanced by nuclide loss by radioactive decay and surface erosion during ice-free periods; i.e. surface nuclide concentrations vary cyclically, but always return to the same value at the same point in a glacial-interglacial cycle. Given this hypothesis, as well as the assumptions that: i) each glacial-interglacial cycle can be characterized by a constant cycle duration (t_c, here assumed to be 100 000 years) and a fraction of that period (f_b, dimensionless) during which the surface is ice-covered and ii) there is no subglacial erosion, nuclide concentrations at the beginning of a glacial period are given by:

$$N_{26} = \frac{P_{26}}{\lambda_{26} + \frac{\varepsilon}{\Lambda}} \frac{\left(1 - \exp\left[-t_c(1-f_b)\left(\lambda_{26} + \frac{\varepsilon}{\Lambda}\right)\right]\right)}{\left(1 - \exp[-t_c\lambda_{26}] \exp\left[-\frac{\varepsilon t_c(1-f_b)}{\Lambda}\right]\right)} \quad (10)$$

$$N_{10} = \frac{P_{10}}{\lambda_{10} + \frac{\varepsilon}{\Lambda}} \frac{\left(1 - \exp\left[-t_c(1-f_b)\left(\lambda_{10} + \frac{\varepsilon}{\Lambda}\right)\right]\right)}{\left(1 - \exp[-t_c\lambda_{10}] \exp\left[-\frac{\varepsilon t_c(1-f_b)}{\Lambda}\right]\right)} \quad (11)$$

$$N_{21} = \frac{P_{21,sp}\Lambda}{\varepsilon} + \frac{P_{21,\mu-}\Lambda_{\mu-}}{\varepsilon} + \frac{P_{21,\mu fast}\Lambda_{\mu fast}}{\varepsilon}. \quad (12)$$

It is necessary to consider, at least approximately, production by muons for ^{21}Ne but not for the radionuclides. Note that we compute the equilibrium nuclide concentration for the beginning of a glacial period, to be consistent with the idea that Taylor Glacier thickens during interglacials (Higgins *et al.* 2000). For each pair of nuclides, the corresponding pairs of equations can be solved for values of the surface erosion rate during ice-free periods ε (g cm^2 a^{-1}) and the fraction of each glacial cycle spent covered by ice f_b. Of course, it would also be possible to search for values of these two parameters that best fit all three nuclide concentrations simultaneously. However, that would discard information regarding changes in the extent of glaciation over time that can potentially be gained by considering the nuclide pairs separately.

Equations (10)–(12) were solved for samples at Mount DeWitt and East Groin using the non-linear least squares algorithm in MATLAB, and used a linear error propagation approximation with numerical partial differentiation to estimate the uncertainties in inferred values of f_b attributable to measurement uncertainty in nuclide concentrations. The results are shown in Fig. 14. For samples whose nuclide concentrations are in equilibrium with continuous surface exposure (i.e. they plot in the region of continuous exposure on Figs 9, 10 & 11) solving these equations must yield $f_b = 0$ within measurement uncertainty for all nuclide pairs. As discussed above, this is the case for all but the lowest sample at Mount DeWitt and for samples from above 1400 m at East Groin. If the scenario implied by Eqs (10)–(12) is correct, f_b must be greater for samples at lower elevations because the ice sheet cannot advance over higher sites without also covering the lower sites. This is the case at both Mount DeWitt and East Groin. At Mount DeWitt this calculation implies that the lowest site was ice-covered for *c*. 20–40% of each glacial-interglacial cycle, but the adjacent site 50 m higher was almost never covered by ice. At East Groin, f_b values computed from each nuclide pair are similar among closely spaced samples and, as expected, higher at lower elevations. The lowest two sites (near 1320 m) at East Groin were covered by ice for *c*. 50% of each cycle, and the two next highest sites (near 1390 m) were covered by ice 5–40% of the time. Thus, our observations at Mount DeWitt and East Groin are consistent with the hypothesis that the observed nuclide concentrations in low elevation samples reflect an equilibrium between production during ice-free periods and loss by radioactive decay and surface erosion during interglaciations under a scenario of repeated, periodic glacial-interglacial cycles spanning the Pleistocene.

For the lowest four samples at East Groin and the lowest sample at Mount DeWitt, values of f_b obtained by solving Eqs (10)–(12) vary systematically among nuclide pairs: ^{26}Al-^{10}Be pairs imply higher values of f_b than ^{26}Al-^{21}Ne and ^{10}Be-^{21}Ne pairs. A possible explanation for

https://doi.org/10.1017/S0954102014000261 Published online by Cambridge University Press

this relies on the fact that nuclides with shorter half-lives reach equilibrium with a periodic exposure-burial history more rapidly. Therefore, the systematic offset among values of f_b inferred from the various nuclide pairs would be due to the fact that sites were, on average, less commonly covered by ice during the longer time period 'remembered' by the ^{26}Al-^{21}Ne and ^{10}Be-^{21}Ne pairs than during the shorter time period recorded by the ^{26}Al-^{10}Be pair. In other words, this explanation would imply an overall increase in the frequency and/or duration of periods of ice cover in the past several million years. For example, the sample at 1314 m at East Groin has values of f_b of 0.67, 0.6 and 0.5 inferred from the ^{26}Al-^{10}Be, ^{26}Al-^{21}Ne and ^{10}Be-^{21}Ne pairs, respectively. One can reproduce this result by assuming that: i) the bedrock surface eroded at 0.5 m Ma^{-1} when it was ice free, and did not erode when it was ice-covered, ii) at 2.5 Ma, nuclide concentrations had reached equilibrium (as defined by Eqs (10)–(12)) with repeated glacial-interglacial cycles consisting of 10 000 years of ice cover and 90 000 years of exposure, and iii) between 2.5 Ma and the present, the relative duration of ice cover gradually increased so that the most recent cycle consisted of 80 000 years of ice cover and 20 000 years of exposure. Although this is only one of many possible ice cover scenarios that would explain these observations, the idea that we infer lower values of f_b from nuclide pairs that take longer to equilibrate is in general agreement with the idea that ice volume changes had higher amplitude in the late Pleistocene than in the early Pleistocene or Pliocene.

Conclusions

In Beacon Group sandstone bedrock surfaces at two sites in the Dry Valleys, ^{26}Al, ^{10}Be and ^{21}Ne concentrations are most easily explained by the following scenario. First, sites at high elevations: i) were rarely covered by ice, ii) have not been significantly subglacially eroded when covered by ice, and iii) have been steadily and slowly eroding at rates of 0.5–1.5 m Ma^{-1} for at least 1–4 Ma when not covered by ice. Second, sites within *c.* 100 m above the present ice surface elevation experienced similar surface erosion rates when ice-free, but have been repeatedly covered by cold-based glacier ice during many glacial-interglacial cycles. Sites near the present-day margin of the Taylor Glacier have been covered by ice around half of the time. Furthermore, differences in the characteristic frequency and/or duration of ice cover inferred from nuclide pairs that reach equilibrium at different rates is consistent with a Pliocene-to-present increase in the fraction of the time these sites have been covered by ice. Apparent surface erosion rates of 0.5–1.5 m Ma^{-1}, which appear to reflect the relative erodibility of Beacon Group sandstones in the Dry Valleys region, imply that the cosmogenic nuclide concentrations at these sites do not record events significantly predating the Pleistocene.

Nuclide concentrations in granite bedrock at the Quartz Hills, in contrast, have not reached production-erosion equilibrium and show that sites have been covered by ice for an insignificant fraction of their total exposure history. Results from these sites are most easily explained by 4–6 Ma exposure at erosion rates of 5–10 cm Ma^{-1}. The order of magnitude difference in erosion rates between the sandstone sites in the Dry Valleys and the Quartz Hills is presumably the result of either more resistant bedrock, a colder or more arid climate, or both. Regardless, the low-erosion-rate sites in the Quartz Hills preserve a longer record of exposure.

Acknowledgements

This work was supported by the National Science Foundation under grants OPP-0838958 (Balco), OPP-0443535 (Balco), OPP-0229314 (Stone), OPP-0636818 (Stone), and by the Ann and Gordon Getty Foundation. Jaakko Putkonen and Dan Morgan assisted with fieldwork and sample collection in the Dry Valleys. Brenda Hall, Gordon Bromley and Howard Conway assisted with fieldwork and mapping at Reedy Glacier. David Shuster and Tim Becker assisted with the ^{21}Ne measurements. Bob Finkel and Dylan Rood assisted with AMS measurements at LLNL-CAMS. Two anonymous reviewers were extremely helpful in improving some aspects of the text.

Supplementary material

A supplemental table will be found at http://dx.doi.org/10.1017/S0954102014000261.

References

Balco, G., Shuster, D.L., Blard, P.-H., Zimmermann, L. & Stone J.O.H. 2011. Cosmogenic Ne-21 production systematics in quartz inferred from a 25-meter sandstone core. *Mineralogical Magazine*, **75**, 473.

Balco, G., Briner, J., Finkel, R.C., Rayburn, J.A., Ridge, J.C. & Schaefer, J.M. 2009. Regional beryllium-10 production rate calibration for late-glacial northeastern North America. *Quaternary Geochronology*, **4**, 93–107.

Balco, G. & Shuster, D.L. 2009a. Production rate of cosmogenic ^{21}Ne in quartz estimated from ^{10}Be, ^{26}Al, and ^{21}Ne concentrations in slowly eroding Antarctic bedrock surfaces. *Earth and Planetary Science Letters*, **281**, 48–58.

Balco, G. & Shuster, D. 2009b. ^{26}Al–^{10}Be–^{21}Ne burial dating. *Earth and Planetary Science Letters*, **286**, 570–575.

Balco, G., Stone, J.O., Lifton, N.A. & Dunai, T.J. 2008. A complete and easily accessible means of calculating surface exposure ages or erosion rates from ^{10}Be and ^{26}Al measurements. *Quaternary Geochronology*, **3**, 174–195.

Bierman, P., Marsella, K., Patterson, C., Davis, P. & Caffee, M. 1999. Mid-Pleistocene cosmogenic minimum-age limits for pre-Wisconsinan glacial surfaces in southwestern Minnesota and southern Baffin Island: a multiple nuclide approach. *Geomorphology*, **27**, 25–39.

Bromley, G.R.M., Hall, B.L., Stone, J.O., Conway, H. & Todd, C.E. 2010. Late Cenozoic deposits at Reedy Glacier, Transantarctic Mountains: implications for former thickness of the West Antarctic Ice Sheet. *Quaternary Science Reviews*, **29**, 384–398.

Brook, E.J. & Kurz, M.D. 1993. Surface-exposure chronology using *in situ* cosmogenic ^{3}He in Antarctic quartz sandstone boulders. *Quaternary Research*, **39**, 1–10.

Chmeleff, J., von Blanckenburg, F., Kossert, K. & Jakob, D. 2009. Determination of the ^{10}Be half-life by multicollector ICP-MS and liquid scintillation counting. *Nuclear Instruments and Methods in Physics Research - Beam Interactions with Materials and Atoms*, **268B**, 192–199.

Fernandez-Mosquera, D., Hahm, D. & Marti, K. 2010. Calculated rates of cosmic ray muon-produced Ne in subsurface quartz. *Geophysical Research Letters*, **37**, 10.1029/2010GL044106.

Granger, D.E. 2006. A review of burial dating methods using ^{26}Al and ^{10}Be. *Geological Society of America Special Paper*, **415**, 1–16.

Heisinger, B., Lal, D., Jull, A.J.T., Kubik, P., Ivy-Ochs, S., Knie, K. & Nolte, E. 2002a. Production of selected cosmogenic radionuclides by muons: 2. Capture of negative muons. *Earth and Planetary Science Letters*, **200**, 357–369.

Heisinger, B., Lal, D., Jull, A.J.T., Kubik, P., Ivy-Ochs, S., Neumaier, S., Knie, K., Lazarev, V. & Nolte, E. 2002b. Production of selected cosmogenic radionuclides by muons: 1. Fast muons. *Earth and Planetary Science Letters*, **200**, 345–355.

Higgins, S.H., Hendy, C.H. & Denton, G.H. 2000. Geochronology of Bonney Drift, Taylor Valley, Antarctica: evidence for interglacial expansions of Taylor Glacier. *Geografiska Annaler - Physical Geography*, **82A**, 391–409.

Klein, J., Giegengack, R., Middleton, R., Sharma, P., Underwood, J.R. & Weeks, R.A. 1986. Revealing histories of exposures using *in situ* produced ^{26}Al and ^{10}Be in Libyan desert glass. *Radiocarbon*, **28**, 547–555.

Korschinek, G., & 13 others. 2010. A new value for the half-life of Be-10 by heavy-ion recoil detection and liquid scintillation counting. *Nuclear Instruments and Methods in Physics Research B - Beam Interactions with Materials and Atoms*, **268**, 10.1016/j.nimb.2009.09.020.

Lal, D. 1991. Cosmic ray labeling of erosion surfaces: *in situ* nuclide production rates and erosion models. *Earth and Planetary Science Letters*, **104**, 424–439.

Liu, H., Jezek, K., Li, B. & Zhao, Z. 2001. *Radarsat Antarctic mapping project digital elevation model* version 2. Technical Report. Boulder, CO: National Snow and Ice Data Center.

Mercer, J.H. 1968. Glacial geology of the Reedy Glacier area, Antarctica. *Geological Society of America Bulletin*, **79**, 471–486.

Middleton, J.L., Ackert, R.P. & Mukhopadhyay, S. 2012. Pothole and channel system formation in the McMurdo Dry Valleys of Antarctica: new insights from cosmogenic nuclides. *Earth and Planetary Science Letters*, **355–356**, 341–350.

Mukhopadhyay, S., Ackert, R.D., Pope, A.E., Pollard, D. & DeConto, R.M. 2012. Miocene to recent ice elevation variations from the interior of the West Antarctic Ice Sheet: constraints from geologic observations, cosmogenic nuclides and ice sheet modeling. *Earth and Planetary Science Letters*, **337–338**, 243–251.

Niedermann, S., Graf, T. & Marti, K. 1993. Mass spectrometric identification of cosmic-ray-produced neon in terrestrial rocks with multiple neon components. *Earth and Planetary Science Letters*, **118**, 65–73.

Nishiizumi, K. 2004. Preparation of ^{26}Al AMS standards. *Nuclear Instruments and Methods in Physics Research - Beam Interactions with Materials and Atoms*, **223–224B**, 388–392.

Nishiizumi, K., Lal, D., Klein, J., Middleton, R. & Arnold, J.R. 1986. Production of ^{10}Be and ^{26}Al by cosmic rays in terrestrial quartz *in situ* and implications for erosion rates. *Nature*, **319**, 134–136.

Stone, J. 2001. *Extraction of Al and Be from quartz for isotopic analysis*. Seattle, WA: UW Cosmogenic Nuclide Lab Methods and Procedures, Available at: http://depts.washington.edu/cosmolab/chem/Al-26_Be-10.pdf.

Sugden, D. & Denton, G. 2004. Cenozoic landscape evolution of the Convoy Range to Mackay Glacier area, Transantarctic Mountains: onshore to offshore synthesis. *Geological Society of America Bulletin*, **116**, 840–857.

Sugden, D.E., Balco, G., Cowdery, S.G., Stone, J.O. & Sass, L.C. 2005. Selective glacial erosion and weathering zones in the coastal mountains of Marie Byrd Land, Antarctica. *Geomorphology*, **67**, 317–334.

Sugden, D.E., Summerfield, M.A., Denton, G.H., Wilch, T.I., McIntosh, W.C., Marchant, D.R. & Rutford, R.H. 1999. Landscape development in the Royal Society Range, southern Victoria Land, Antarctica: stability since the mid-Miocene. *Geomorphology*, **28**, 181–200.

Todd, C., Stone, J., Conway, H., Hall, B. & Bromley, G. 2010. Late Quaternary evolution of Reedy Glacier, Antarctica. *Quaternary Science Reviews*, **29**, 1328–1341.